

# Geophysical Research Letters®

## RESEARCH LETTER

10.1029/2022GL100003

### Key Points:

- We present a 17 kyr record of foraminiferal Nd isotopes from the intermediate-depth northern Indian Ocean with a resolution of ~200 years
- Both regional Himalayan weathering inputs and intermediate water advection from the Southern Ocean influenced the record
- Different interhemispheric relationships are revealed between Antarctic Intermediate Water and the Indian Summer Monsoon during the last deglaciation compared to the Early Holocene

### Supporting Information:

Supporting Information may be found in the online version of this article.

### Correspondence to:






Z. Yu,  
yuzhaojie@qdio.ac.cn

### Citation:

Yu, Z., Colin, C., Wilson, D. J., Bayon, G., Song, Z., Sepulcre, S., et al. (2022). Millennial variability in intermediate ocean circulation and Indian monsoonal weathering inputs during the last deglaciation and Holocene. *Geophysical Research Letters*, 49, e2022GL100003. <https://doi.org/10.1029/2022GL100003>

Received 10 JUN 2022  
Accepted 25 OCT 2022

## Millennial Variability in Intermediate Ocean Circulation and Indian Monsoonal Weathering Inputs During the Last Deglaciation and Holocene

Zhaojie Yu<sup>1,2,3</sup> , Christophe Colin<sup>4</sup>, David J. Wilson<sup>5</sup> , Germain Bayon<sup>6</sup>, Zehua Song<sup>1</sup> , Sophie Sepulcre<sup>4</sup> , Arnaud Dapoigny<sup>7</sup>, Yuanlong Li<sup>8</sup>, and Shiming Wan<sup>1,2,3</sup> 

<sup>1</sup>Key Laboratory of Marine Geology and Environment, Institute of Oceanology, Chinese Academy of Sciences, Qingdao, China, <sup>2</sup>Laboratory for Marine Geology, Qingdao National Laboratory for Marine Science and Technology, Qingdao, China, <sup>3</sup>Center for Ocean Mega-Science, Chinese Academy of Sciences, Qingdao, China, <sup>4</sup>Université Paris-Saclay, CNRS, GEOPS, Orsay, France, <sup>5</sup>Institute of Earth and Planetary Sciences, University College London and Birkbeck, University of London, London, UK, <sup>6</sup>IFREMER, Marine Geoscience Unit, Plouzané, France, <sup>7</sup>LSCE/IPSL, CEA-CNRS-UVSQ, Université Paris-Saclay, Gif-sur-Yvette, France, <sup>8</sup>Key Laboratory of Ocean Circulation and Waves, Institute of Oceanology, Chinese Academy of Sciences, Qingdao, China

**Abstract** The relationship between ocean circulation and monsoon systems over orbital to sub-millennial timescales is a crucial but poorly constrained component of the climate system. Here, using foraminiferal and detrital neodymium (Nd) isotope records from the intermediate-depth northern Indian Ocean, we provide new evidence revealing that both monsoon-driven weathering inputs and water mass advection from the Southern Ocean influenced past seawater Nd isotope changes in this region. Our results suggest that Indian Summer Monsoon weakening coincided with enhanced northward Antarctic Intermediate Water (AAIW) advection during the last deglaciation, reflecting a strong interhemispheric coupling. In contrast, the Early Holocene was characterized by enhanced monsoon strength but persistently strong AAIW inflow, indicating a relationship in the opposite sense. These differing interhemispheric relationships indicate asynchronous changes in the global atmosphere—ocean—climate system, and may represent a previously unrecognized component of the ocean-atmosphere reorganization during the deglacial to Holocene transition.

**Plain Language Summary** Deciphering the interactions between processes in the Northern and Southern hemispheres is crucial for understanding the mechanisms of paleoclimate change, and therefore for predicting future climate evolution. Resolving the nature of such interactions requires high-resolution datasets from key components of the system. To this end, we present a new intermediate-depth foraminiferal neodymium (Nd) isotope record from the Indian Ocean covering the last 17,000 years at an unprecedented resolution of ~200 years. Variability in this Nd isotope record reflects both changes in regional Nd inputs related to continental weathering driven by the Indian Summer Monsoon (ISM), and changes in the Nd signal carried northwards from the Southern Ocean by Antarctic Intermediate Water (AAIW). By disentangling these continental weathering and ocean circulation signals, we can compare Northern and Southern Hemisphere climate processes on sub-millennial timescales. We found that ISM weakening coincided with enhanced northward AAIW advection during the last deglaciation, whereas enhanced monsoonal activity was accompanied by persistently strong intermediate water inflow during the Early Holocene. This variable interhemispheric connection between the summer monsoon and intermediate water advection may have played a crucial role in the last deglacial climate transition.

## 1. Introduction

Paleoclimate records indicate that the evolution of the Indian Summer Monsoon (ISM) over orbital timescales is not only controlled by Northern Hemisphere insolation forcing, but is also sensitive to internal Earth system processes involving interhemispheric interactions (Bolton et al., 2013; Caley et al., 2011; Clemens & Prell, 2003). On millennial timescales, changes in the ISM intensity appear to be synchronous with North Atlantic Heinrich events (Kathayat et al., 2016), with weakening of the ISM possibly induced by southward migration of the Intertropical Convergence Zone (Deplazes et al., 2014; Nilsson-Kerr et al., 2019) and sea surface cooling in the northern Indian Ocean (Tierney et al., 2015) during these North Atlantic cold periods. Such variations of the ISM across orbital to millennial timescales suggest that it could represent a key player in the interhemispheric

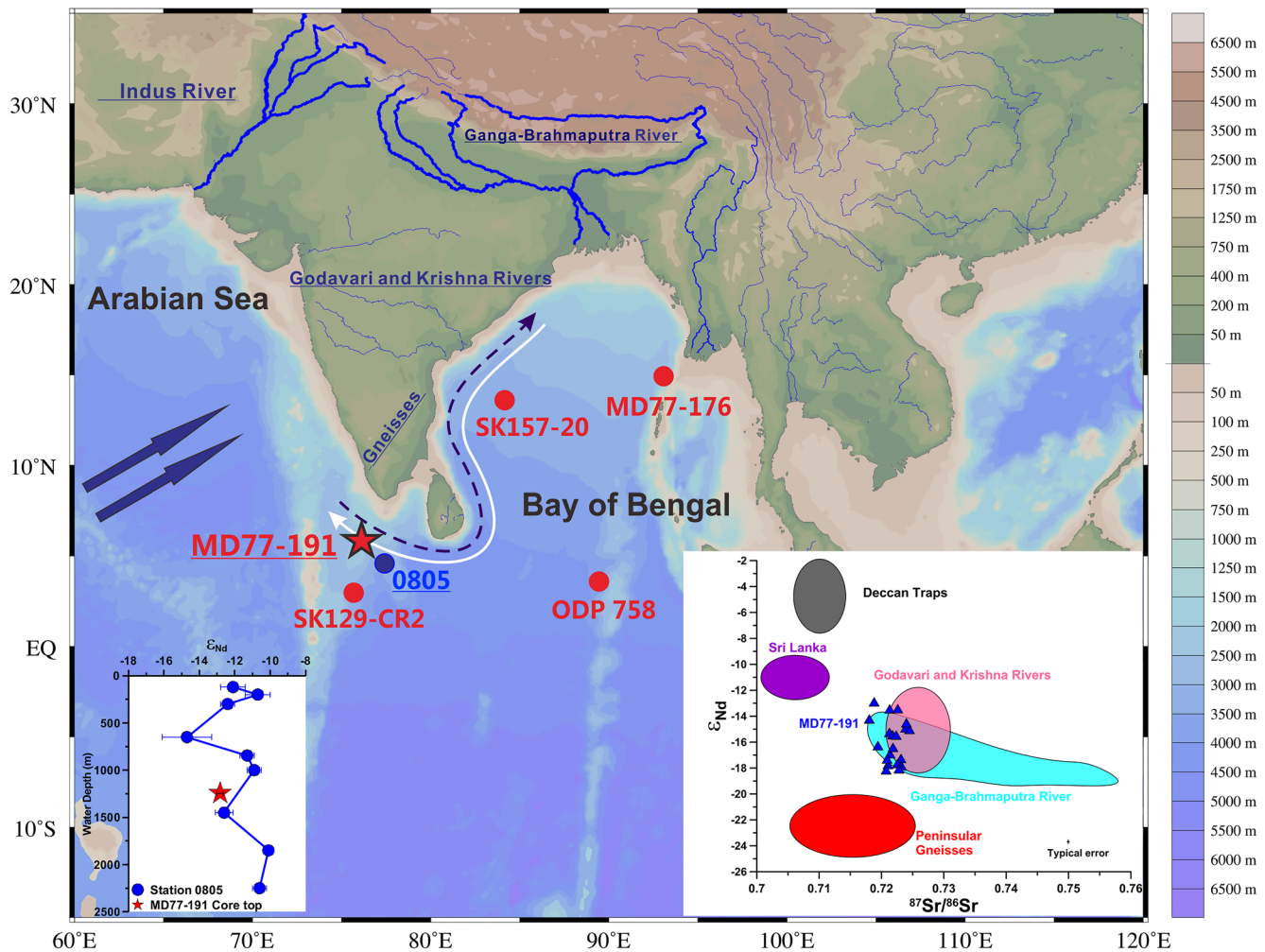


**Figure 1.** Bathymetric map showing the location of core MD77-191 (red star) and other core sites discussed in this study (red circles). Seawater Nd isotope profile (blue circle) is from station 0805. Indian Summer Monsoon (ISM) is marked schematically with blue arrows. White and black arrows indicate seasonal reversals in the East India Coastal Current related to the ISM (white solid line = winter; black dashed line = summer). Inset figure in the bottom-left shows that the core top foraminifera Nd isotope composition in core MD77-191 is consistent with the seawater Nd isotope profile at the depth of this core from station 0805 (Goswami et al., 2014) (error bars are  $2\sigma$  uncertainty). Inset figure in the bottom-right is a cross plot of  $\epsilon_{Nd}$  values versus  $^{87}Sr/^{86}Sr$  ratios in detrital sediments from core MD77-191 (blue triangles, this study) compared to potential sediment sources: Ganga-Brahmaputra River (Lupker et al., 2013; Singh & France-Lanord, 2002), Godavari and Krishna Rivers (Ahmad et al., 2009), Deccan Traps (Dessert et al., 2001; Lightfoot & Hawkesworth, 1988), Peninsular Gneisses (Goswami et al., 2012), and Sri Lanka (Perera & Kagami, 2011). Typical error bar represents  $2\sigma$  uncertainty.

interactions, while also possibly exerting feedback on climate change through continental weathering inputs of alkalinity and nutrients to the ocean (Vance et al., 2009). In order to better decipher past changes in the ISM and inform on likely changes in the future, high-resolution proxies that are sensitive to atmospheric and ocean circulation are required to resolve the physical processes involved in interhemispheric coupling linked to the ISM.

Here, we present a new high-resolution deglacial and Holocene Nd isotope record generated using 25–30 mg of  $>150 \mu m$  size fraction of mixed planktic foraminifera in the northern Indian Ocean core MD77-191 ( $7^{\circ}30' N$ ,  $76^{\circ}43' E$ , 1,254 m, Figure 1). The Nd isotopic composition (expressed as  $\epsilon_{Nd}$ , see Materials and methods in Supporting Information S1) of seawater near ocean margins is spatially variable, with past variability reflecting a combination of both regional changes in the rate or mode of continental weathering and changes in water mass mixing related to regional or global-scale ocean circulation (Goldstein & Hemming, 2003; van de Flierdt et al., 2016). Neodymium is incorporated post-mortem into foraminiferal coatings from bottom waters and/or pore fluids, and this signal overwhelms any Nd acquired by foraminifera in surface waters (Tachikawa et al., 2014), so our record constrains past bottom water compositions at the core site (see also Materials and methods in

Supporting Information S1). In this region, the Nd isotopic composition of ISM-induced Himalayan weathering inputs ( $\epsilon_{\text{Nd}} \sim -18$  to  $-14$ ) (Galy & France-Lanord, 2001; Lupker et al., 2013; Singh & France-Lanord, 2002) is highly distinct from the composition of intermediate water masses originating in the Southern Ocean (mainly Antarctic Intermediate Water: AAIW,  $\epsilon_{\text{Nd}} \sim -9$  to  $-7$ ; Amakawa et al., 2019; van de Flierdt et al., 2016), making Nd isotopes a sensitive tracer of past weathering changes (Burton & Vance, 2000; Gourlan et al., 2010; Yu et al., 2018) as well as ocean circulation changes. We additionally measured strontium (Sr) and Nd isotopes on the clay size fraction ( $<2 \mu\text{m}$ ) of the detrital sediment to provide complementary evidence on changes in the erosional system (see Materials and methods in Supporting Information S1).

Core MD77-191 is well-suited to record changes of ISM-induced weathering inputs and intermediate ocean circulation for several reasons: (a) its high sedimentation rate enables an unprecedented high resolution ( $\sim 200$  yr) foraminiferal Nd isotope record that resolves millennial and sub-millennial changes; (b) it is located beyond the limits of the main Bengal Fan and therefore should record a representative regional signal of Himalayan weathering inputs; (c) it records changes in the intermediate ocean, which is more sensitive to Himalayan inputs than the deep ocean, as indicated by a modern seawater Nd isotope study (Yu et al., 2017); and (d) deglacial Nd isotope end-member changes in Southern Ocean intermediate waters were modest (Hu et al., 2016). While slightly more radiogenic Nd isotope values have been inferred for AAIW in the South Atlantic and South Pacific during the last deglaciation than the Holocene (Hu et al., 2016), these changes were small relative to the Nd isotope changes recorded in core MD77-191.

Terrestrial weathering in the Himalaya is directly related to the ISM and its associated precipitation patterns, which are influenced by North Atlantic climate oscillations on millennial timescales (Hein et al., 2017; Lupker et al., 2013). In contrast, variations in the invasion of AAIW into the northern Indian Ocean are expected to be controlled by Southern Hemisphere processes, including the sinking of surface waters at the Antarctic Polar Front and the intensity of the westerly winds that influence AAIW formation and its northward transport (Anderson et al., 2009; Hillenbrand et al., 2017; Yu et al., 2018). Both these mechanisms (i.e., the ISM and the AAIW) have separately played an important role in millennial-scale climate variability and associated interhemispheric interactions (Anderson et al., 2009; Tierney et al., 2015).

## 2. Results and Discussion

### 2.1. Detrital Sediment Provenance at Site MD77-191

By analyzing the clay size component ( $<2 \mu\text{m}$ ) of the MD77-191 detrital sediments (see Materials and methods; Table S2 in Supporting Information S1), possible grain size effects on Nd and Sr isotopic compositions are minimized (Lupker et al., 2013). The  $\epsilon_{\text{Nd}}$  values and  $^{87}\text{Sr}/^{86}\text{Sr}$  ratios in core MD77-191 range from  $-18.1$  to  $-12.9$  (average  $-15.9$ ) and  $0.7180$  to  $0.7245$  (average  $0.7218$ ), respectively (Figure 1). Comparison to potential source compositions indicates that the clay-size fractions in core MD77-191 were derived from mixing between sediments exported from the Ganga-Brahmaputra and eastern Indian river systems (Godavari and Krishna Rivers), which were further transported to the study site via the East India Coastal Current (Figure 1). In turn, the Sahyadri mountains (Western Ghats) are the main sediment source that supplies the eastern Indian rivers.

The detrital Nd isotope record in core MD77-191 generally shows more radiogenic values during the last deglaciation ( $\epsilon_{\text{Nd}} = -15.4$  to  $-12.9$ ) than during the Holocene ( $\epsilon_{\text{Nd}} = -18.1$  to  $-16.3$ ), as well as revealing deglacial millennial-scale variability (Figure 2). It is important to note that the Nd isotopic composition of regional-scale detrital inputs from the Ganga-Brahmaputra and eastern Indian rivers have remained largely unchanged during the last deglaciation and Holocene periods (Ahmad et al., 2009; Galy & France-Lanord, 2001; Lupker et al., 2013; Singh & France-Lanord, 2002). Therefore, rather than recording Nd isotope end-member changes within those river systems, the observed detrital Nd isotope variability in core MD77-191 most likely reflects changes in mixing proportions between Ganga-Brahmaputra and eastern Indian river sediment sources. Such orbital and millennial-scale changes in the sediment sources could be attributed to changes in the ISM precipitation, which was notably weakened during Heinrich Stadial 1 (HS1) and the Younger Dryas (YD; Dutt et al., 2015; Kudrass et al., 2001, see also Figure S6 in Supporting Information S1).

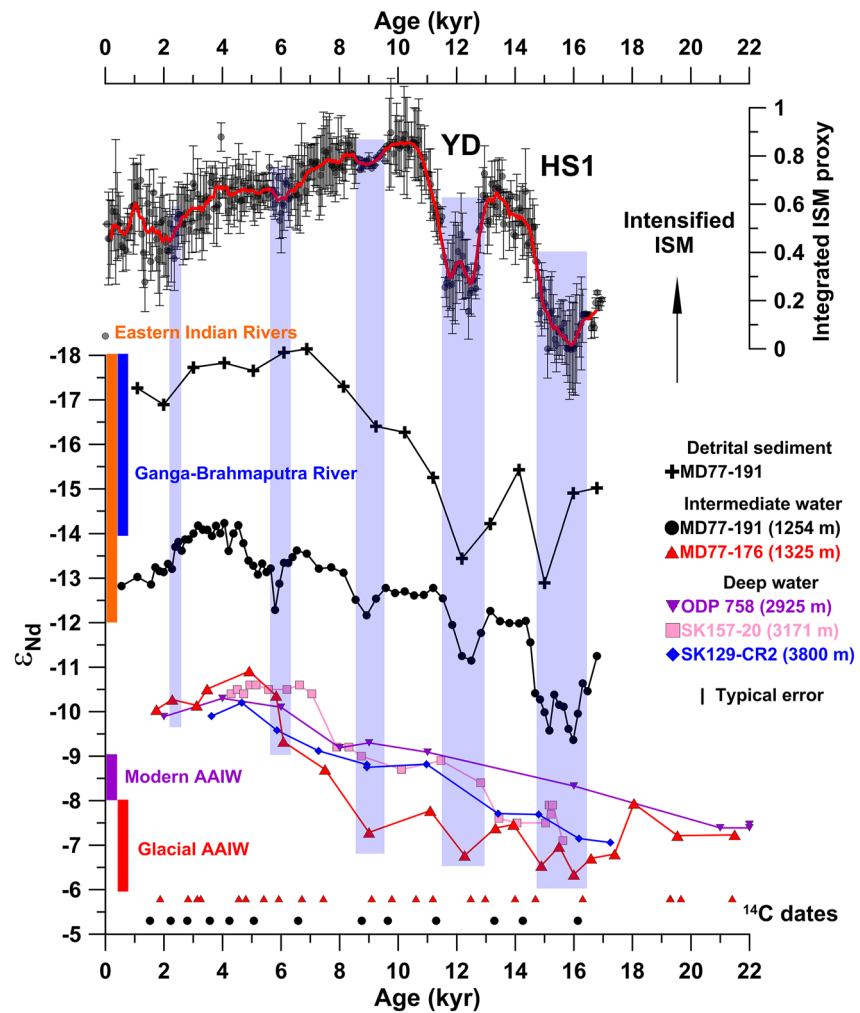


**Figure 2.** Comparison of foraminiferal and detrital Nd isotope records from core MD77-191 to existing seawater Nd isotope records from the northern Indian Ocean and the integrated Indian Summer Monsoon (ISM) proxy. Intermediate water Nd isotope records are from MD77-191 (this study) and MD77-176 (Yu et al., 2018). Deep water Nd isotope records are from ODP 758 (Burton & Vance, 2000), SK157-20 (Naik et al., 2019), and SK129-CR2 (Wilson, Piotrowski, et al., 2015). Blue bars indicate the consistent millennial-scale variations during HS1, the YD, and the Holocene. Colored bars along the Nd isotope axis indicate the end-members influencing core MD77-191: modern and glacial AAIW (purple and red; Amakawa et al., 2019; Hu et al., 2016; van de Flierdt et al., 2016), and weathering inputs from the Ganga-Brahmaputra River (blue) and eastern Indian rivers (orange; see Figure 1 for references). Typical error bar represents  $2\sigma$  uncertainty for Nd isotope analyses. The integrated ISM proxy record is plotted as gray circles, with a temporally varying error calculated using the double standard deviation of the overlapped intervals, while the red curve is a running mean with a window width of 9 (see Figures S4–S6 in Supporting Information S1 for details on the ISM proxy).

## 2.2. Millennial Variability of Seawater Nd Isotopes in the Northern Indian Ocean

A late Holocene core-top foraminifera sample in core MD77-191 has an  $\epsilon_{Nd}$  value of  $-12.8 \pm 0.2$  ( $2\sigma$ ), consistent with modern seawater measurements from a similar water depth at nearby station 0805 ( $\epsilon_{Nd} = -12.6 \pm 0.5$ ; Figure 1; Goswami et al., 2014). This observation provides support for the extraction of a reliable bottom-water Nd isotope signature using planktic foraminifera at the studied site. While dissolved-particulate exchange processes and porewater imprints can impact the authigenic  $\epsilon_{Nd}$  signature extracted from marine sediments at continental margins (Abbott et al., 2022; Blaser et al., 2019; Wilson et al., 2012), these effects are likely to scale with sediment reactivity and detrital sedimentation rates (Abbott et al., 2022; Blaser et al., 2019), which are expected to have remained near-constant over the last 17 kyr in this setting (Figure S1 in Supporting Information S1). In contrast, the studies of Abbott et al. (2022) and Blaser et al. (2019) are from high-latitude North Atlantic cores that were influenced by either significant inputs of reactive volcanics from Iceland (with highly



radiogenic Nd isotope signatures, which are not seen in core MD77-191), or by temporally varying inputs of glacial flour or detrital carbonates in Heinrich layers. Moreover, similar long-term variations of authigenic Nd isotopes have been observed in several cores from the Bay of Bengal (Figure 2), which were characterized by different lithologies, sedimentation rates, and detrital Nd isotope evolution patterns (Figure S2 in Supporting Information S1). Therefore, we interpret those authigenic Nd isotope records in terms of a regional seawater signal, and not as the product of local diagenesis. The measured values are best interpreted as reflecting the combined influence of intermediate waters advected from the Southern Ocean (AAIW;  $\epsilon_{\text{Nd}} \sim -9$  to  $-7$ ; Amakawa et al., 2019; van de Flierdt et al., 2016) and regional dissolved Nd inputs derived from the Ganga-Brahmaputra (Singh & France-Lanord, 2002) and eastern Indian rivers (Ahmad et al., 2009), characterized by significantly less radiogenic Nd isotope signatures (Figure 2). Such an explanation is also supported by mass-balance modeling conducted at seawater station 0805 (Goswami et al., 2014), which provides evidence for dissolved Nd excesses in modern intermediate waters linked to a regional sediment end-member with  $\epsilon_{\text{Nd}}$  values in the range of  $-18$  to  $-14$  (Figure 1).

The reconstructed intermediate water  $\epsilon_{\text{Nd}}$  values in core MD77-191 range from  $-14.2$  to  $-9.4$  ( $\pm 0.2$ ), displaying a broadly similar long-term evolution to existing deglacial and Holocene Nd isotope records from the Bay of Bengal (Burton & Vance, 2000; Naik et al., 2019; Wilson, Piotrowski, et al., 2015; Yu et al., 2018; Figure 2; Table S1 in Supporting Information S1). All these records show a decrease in  $\epsilon_{\text{Nd}}$  values from the end of the last glacial period to the Early/Middle Holocene, followed by a small increase toward the present day. In detail, the deep sites record total variability of  $\sim 3$   $\epsilon_{\text{Nd}}$  units, while the two records from intermediate depths (cores MD77-191 and MD77-176) display larger temporal changes of  $\sim 5$   $\epsilon_{\text{Nd}}$  units, which cannot be explained by differences in sample resolution (Figure 2). This scenario differs from Southern Ocean variability over this interval, where larger Nd isotope changes were recorded in the deep ocean than in the intermediate ocean (Hu et al., 2016). It should be noted that the absolute values differ by  $\sim 4$   $\epsilon_{\text{Nd}}$  units between the two intermediate depth records from cores MD77-191 and MD77-176, presumably due to the influence of radiogenic inputs from the Irrawaddy River and the proximal Indo-Burman Ranges at the location of core MD77-176 (Yu et al., 2018), whereas the record from core MD77-191 predominantly reflects unradiogenic inputs from the Himalaya and eastern India (Figures 1 and 2). In addition, an important new observation is that core MD77-191 clearly records millennial variability in Nd isotopes, while such variations are not seen in the deep ocean records (Figure 2).

### 2.3. Weathering Variations Linked to the ISM

To compare our Nd isotope record with ISM rainfall intensity, we compiled stalagmite  $\delta^{18}\text{O}$  data from a total of 14 caves spanning  $0^\circ$ – $35^\circ\text{N}$ ,  $70^\circ$ – $95^\circ\text{E}$  to establish a continuous integrated ISM proxy record for the last 17 kyr (Supporting Information S1; Comas-Bru et al., 2020; Liu et al., 2020). Stalagmite  $\delta^{18}\text{O}$  records from the ISM-dominated region provide a robust proxy for changes in ISM rainfall, although the extent to which they quantitatively reflect precipitation amount remains debated (Liu et al., 2020). Importantly, the correspondence between the integrated ISM proxy record and both the Chinese cave stalagmite  $\delta^{18}\text{O}$  records (Cheng et al., 2016) and other independent monsoon indicators from the marine realm (Contreras-Rosales et al., 2014; Kudrass et al., 2001) supports its utility (Figure S6 in Supporting Information S1).

Over millennial timescales, the Nd isotope variability in core MD77-191 is similar to changes in the ISM rainfall intensity, as inferred from the integrated ISM proxy record (Figure 2). In particular, abrupt shifts toward radiogenic Nd isotope values during HS1 and the YD, and to a lesser extent during some discrete Holocene events at approximately 9, 6, and 2.5 ka, coincide closely with periods of weakening in the ISM (Figure 2).

A first hypothesis to explain the link between our foraminiferal Nd isotope record and ISM variability is that it could have arisen from changes in the mixing proportions between dissolved inputs from the Ganga-Brahmaputra and eastern Indian rivers. However, a hypothesis that explains our foraminiferal record only by changes in the mixing proportions of these rivers, but with no changes in their weathering fluxes, is not viable for two main reasons. First, there is independent evidence that South Asian riverine discharges significantly increased during the Early Holocene, accompanied by an intensification of monsoon precipitation (Kudrass et al., 2001; Lupker et al., 2013; Nilsson-Kerr et al., 2019). Second, the significant offset ( $\sim 2$  to  $5$   $\epsilon_{\text{Nd}}$  units) between the foraminiferal and detrital Nd isotope curves (Figure 2) requires a radiogenic Nd source to the local seawater, which is assumed to

correspond to southern-sourced waters ( $\epsilon_{Nd} \sim -9$  to  $-7$ ; Amakawa et al., 2019; van de Flierdt et al., 2016). Below, we consider a mass balance approach using the weathering inputs and southern-sourced waters as end-members:

$$\epsilon_{Nd_w} [Nd]_w + \epsilon_{Nd_s} [Nd]_s = \epsilon_{Nd_A} ([Nd]_w + [Nd]_s) \quad (1)$$

where  $\epsilon_{Nd_w}$ ,  $\epsilon_{Nd_s}$ , and  $\epsilon_{Nd_A}$  correspond to the Nd isotopic compositions of regional weathering inputs, southern-sourced waters, and measured foraminiferal values in core MD77-191, respectively. The terms  $[Nd]_w$  and  $[Nd]_s$  represent Nd fluxes for the regional weathering inputs and southern-sourced waters that contributed to the authigenic Nd budget of the measured foraminiferal fractions. The average compositions of regional detrital inputs ( $\epsilon_{Nd_w}$ ) and foraminifera ( $\epsilon_{Nd_A}$ ) in core MD77-191 are approximately  $-16$  and  $-12$ , respectively, while the southern-sourced water end-member ( $\epsilon_{Nd_s}$ ) is approximately  $-8$  (Amakawa et al., 2019; van de Flierdt et al., 2016). From this equation, we calculate that  $[Nd]_w$  should be approximately equal to  $[Nd]_s$ , indicating that the weathering inputs and Nd advected in AAIW play comparable roles in the Nd budget. Therefore, considering a  $5 \epsilon_{Nd}$ -unit change in the regional weathering end-member as a likely maximum (based on the detrital sediment record in core MD77-191), it is clear that a change in this end-member cannot account for the full magnitude of the  $\epsilon_{Nd}$  variability reconstructed for the seawater composition ( $\sim 5 \epsilon_{Nd}$  units).

Studies using the elemental geochemistry of detrital sediments (Lupker et al., 2013; Miriyala et al., 2017) and stable isotopes of terrestrial plant wax compounds (Hein et al., 2017) have demonstrated that the chemical weathering intensity in the Himalayan system increased considerably since the Last Glacial Maximum, and was tied to increased ISM intensity. However, those studies mostly constrain changes in weathering intensity rather than fluxes, or provide first-order estimates of glacial-interglacial changes in weathering fluxes assuming a steady state for sediment fluxes, which involves large uncertainties of up to an order of magnitude (Lupker et al., 2013). Hence, our record, in directly responding to dissolved weathering fluxes through time, is highly complementary in demonstrating that Himalayan weathering fluxes increased from glacial to interglacial periods, and also that they varied over millennial timescales.

Based on evidence from marine beryllium isotope records ( $^{10}\text{Be}/^9\text{Be}$ ), it has recently been proposed that global riverine runoff and weathering fluxes remained near constant during the Cenozoic era and its associated global cooling (Lenard et al., 2020; Willenbring & von Blanckenburg, 2010), and through Pleistocene glacial-interglacial cycles (von Blanckenburg et al., 2015), although with spatially variable patterns. In contrast, both the integrated ISM proxy and foraminiferal Nd isotope data in core MD77-191 are inconsistent with those findings, suggesting instead that dramatic changes in weathering fluxes occurred in the past in response to climate variability, at least during the last deglacial climate transition. As such, our new record provides important evidence on the variability in chemical weathering in this region over orbital timescales, which appears to be missed in some modeling approaches (von Blanckenburg et al., 2015).

Our new Nd isotope record also provides evidence that continental weathering fluxes in tropical monsoon regions can be highly sensitive to climate change on millennial timescales. Previous studies highlighted that deglacial inputs of glacial rock flour in high latitudes (Foster & Vance, 2006; Zhao et al., 2019) and variations in exposed continental area forced by changes in sea level (Foster & Vance, 2006; von Blanckenburg et al., 2015) could potentially dominate past changes in weathering fluxes to seawater. Our data are insensitive to such factors, because of the short (millennial) timescales involved and the persistence of the link between chemical weathering and climate forcing through the deglaciation and the Holocene (Figure 2). Therefore, not only do our results support previous suggestions that climate forcing from the ISM exerts a dominant control on catchment-scale chemical weathering during late Pleistocene glacial-interglacial cycles (Burton & Vance, 2000; Gourelan et al., 2010; Wilson, Galy, et al., 2015), but we now extend that conclusion to millennial timescales.

#### 2.4. Influence of Southern-Sourced Water Variability

Although the Nd isotope record from core MD77-191 and the integrated ISM proxy show close agreement on millennial timescales, there are some inconsistencies in their long-term trends, particularly during the Holocene (Figures 2 and 3). The Early Holocene was characterized by intensified ISM precipitation compared to the Late Holocene (Figures 2 and 3c; Contreras-Rosales et al., 2014; Kaushal et al., 2018), which led to enhanced riverine export of lithogenic material to the northern Indian Ocean (Lupker et al., 2013). In contrast, foraminiferal Nd isotopes in core MD77-191 gradually evolved toward unradiogenic values following the deglaciation (Figures 2

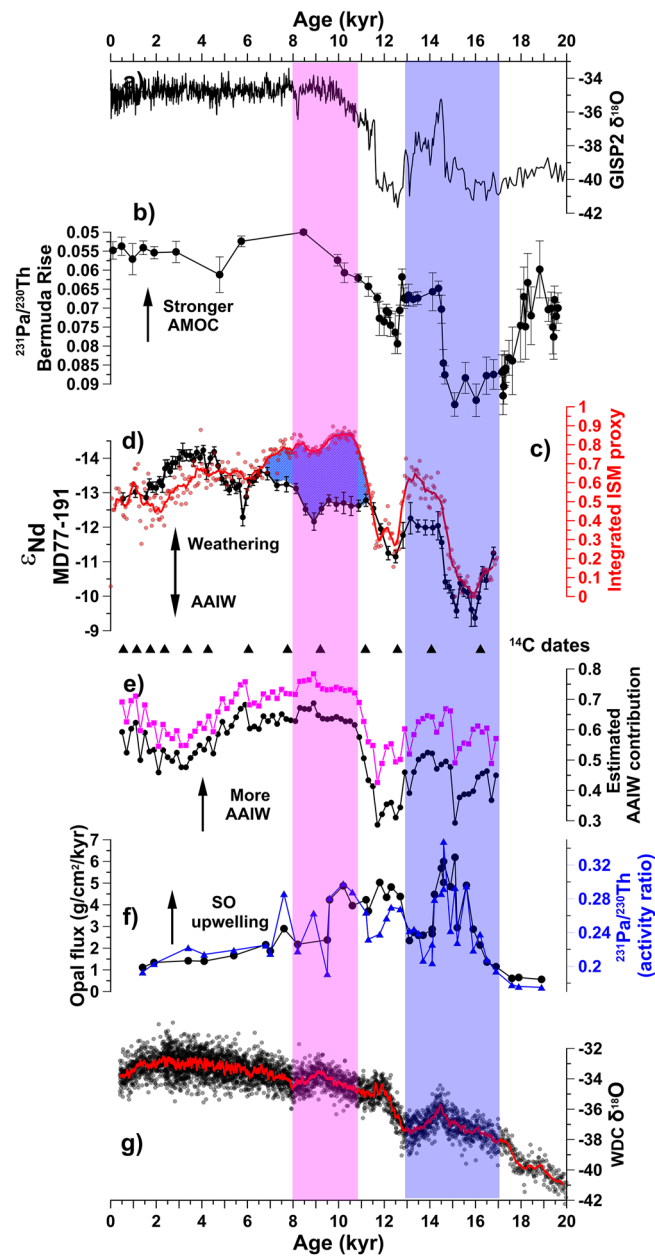


**Figure 3.** Chemical weathering and Antarctic Intermediate Water (AAIW) proxies in core MD77-191 compared to Northern and Southern Hemisphere climate records. (a) Greenland ice core  $\delta^{18}\text{O}$  record from GISP2 (Grootes & Stuiver, 1997). (b) Atlantic meridional overturning circulation (AMOC) intensity indicated by  $^{231}\text{Pa}/^{230}\text{Th}$  excess at Bermuda Rise (McManus et al., 2004). (c) Integrated ISM proxy (this study; red line is a 9-point running mean; see Figures S4–S6 in Supporting Information S1 for details). (d) Nd isotope record from planktic foraminifera in core MD77-191 (this study). Radiocarbon dates in MD77-191 are shown with black triangles below this panel. (e) Estimated AAIW contribution calculated using Nd isotope records from ODP Site 1087 (magenta line) or core Y9 (black line) as the AAIW end-member (this study; see Figures S7–S8 in Supporting Information S1). Note that this sensitivity test indicates similar results for the two different AAIW end-member choices, with an absolute difference of about 10%. (f) Southern Ocean upwelling proxy records (Anderson et al., 2009). (g) Antarctic ice core  $\delta^{18}\text{O}$  record (and 5-point running mean; red line) from WAIS Divide Core (WAIS Divide Project Members, 2013). Blue bar indicates the approximate timing of the deglaciation. Pink bar (and blue shaded area in panels (c–d)) indicates the Early Holocene decoupling between the ISM strength and the MD77-191 Nd isotope record, which is attributed to strengthened AAIW advection. Error bars in panels (b) and (d) are  $2\sigma$  uncertainty.

and 3d), and did not reach an unradiogenic peak until  $\sim 4$  ka, by which time the ISM had already weakened (Figures 3c and 3d). Although we cannot rule out a minor influence on the foraminiferal values from gradual changes in the composition of the weathering inputs (Figure 2), it seems unlikely to have been the major control. In particular, the foraminiferal Nd isotope evolution diverges from the detrital Nd isotope record of core MD177-191 during the Holocene, with the latter reaching a much earlier peak at  $\sim 7$  ka (Figure 2), more consistent with changes in the ISM.

In order to estimate changes through time in the influence of AAIW advection, we applied a two end-member mixing model (Equation 1) to our foraminiferal Nd isotope record for core MD77-191 (see Supporting Information S1). Specifically, we used the integrated ISM proxy as an indicator of regional weathering input fluxes of Nd, the detrital Nd isotope record in core MD77-191 to represent the composition of those weathering inputs, and existing paleoceanographic records to constrain the Nd isotopic composition of the AAIW end-member advected from the Southern Ocean (Hu et al., 2016), from which we calculated the “AAIW contribution” (see Supporting Information S1). Considering the uncertainties in the calculation and its empirical nature, we only interpret it as an indicator of relative (rather than absolute) changes in AAIW contributions (see Supporting Information S1). Nevertheless, in light of only modest changes in AAIW composition close to its Southern Ocean source regions during the deglaciation and even smaller changes during the Holocene (Hu et al., 2016), we argue that it predominantly records a signal of changing AAIW advection (see Supporting Information S1). The most distinct features of the AAIW curve are the strong AAIW contributions during the last deglaciation and the Early Holocene, and a decreasing contribution since the Early Holocene (Figure 3e). Sensitivity tests using different sediment core records as the input for the Nd isotopic composition of the AAIW end-member advected from the Southern Ocean show very similar results (Figure 3e and Figures S7–S8 in Supporting Information S1), indicating that those features are robust results.

At present, AAIW extends northwards to approximately  $20^{\circ}\text{N}$  in the Atlantic and Pacific Oceans, but reaches only as far north as a hydrological front at around  $10^{\circ}\text{S}$  in the Indian Ocean (Talley, 1996). However, compared to the present day, the global intermediate-water circulation during the last deglaciation and the Early Holocene was different. Several studies provide independent support for enhanced production and northward propagation of AAIW during the last deglaciation (Figure S9 and Table S3 in Supporting Information S1), including Nd isotope and radiocarbon records from the Indian Ocean (Bryan et al., 2010; Yu et al., 2018) and Pacific Ocean (Basak et al., 2010; Marchitto et al., 2007). The AAIW invasion identified at Site MD77-191 during the Early Holocene is similar to other significant AAIW fluctuations that occurred during the last deglaciation (Figure 3e), consistent with previous inferences based on intermediate-depth Nd isotope, radiocarbon, and benthic carbon isotope data in other marine sediment core records (Figure S9 and Table S3 in Supporting Information S1).

## 2.5. Variable Deglacial and Holocene Interhemispheric Interactions

Our interpretation of strong AAIW transport during both the last deglaciation and the Early Holocene indicates differences in interhemispheric interactions in the global atmosphere–ocean–climate system. During the last deglaciation, particularly the cold North Atlantic millennial events of HS1 and the YD, the North Atlantic region was cold (Grootes & Stuiver, 1997), the Atlantic meridional overturning circulation was weakened (McManus et al., 2004), and the Intertropical Convergence Zone was shifted southwards, leading to a weakened ISM and reduced riverine Nd inputs from the Himalayan rivers (Figures 3a–3d). Concomitantly, through the bipolar seesaw, the Southern Hemisphere experienced a warming climate (WAIS Divide Project Members, 2013), southward-shifted westerly winds, enhanced Southern Ocean upwelling (Anderson et al., 2009), and strengthened AAIW formation (Figures 3e–3g).

In contrast, such anti-phased behavior between Northern and Southern Hemisphere climates was not apparent during the Early Holocene. During this interval, North Atlantic temperatures and Atlantic meridional overturning circulation strength gradually recovered following the YD (Figures 3a and 3b; Grootes & Stuiver, 1997; McManus et al., 2004), potentially related to strong insolation forcing (Laskar et al., 2004), which drove a northward shift in the Intertropical Convergence Zone, an enhancement of the ISM rainfall (Figure 3c), and increases in riverine inputs to the northern Indian Ocean. Meanwhile, the Southern Hemisphere also warmed slightly (WAIS Divide Project Members, 2013), although with a smaller magnitude than during the deglacial warming events (Figure 3g), and the persistence of Southern Ocean upwelling (Figure 3f; Anderson et al., 2009) indicates that the sea ice extent remained modest. Southward-shifted Southern Hemisphere westerly winds may have



contributed to CDW upwelling during the Early Holocene (Hillenbrand et al., 2017), and such conditions likely supported persistently strong AAIW formation and penetration to the northern oceans.

## 2.6. Implications

Our new finding of a close linkage between terrestrial weathering and the ISM over millennial timescales could be used to provide key boundary conditions for future climate and biogeochemical models. The results of our study also emphasize the need for accurate representation of tropical monsoonal precipitation in climate models, if such outputs are used to model past or future river chemistry and weathering fluxes. Underestimation of glacial-interglacial monsoonal precipitation changes could partly explain discrepancies between the minimal changes in chemical weathering fluxes predicted for the Himalayan system in some models (von Blanckenburg et al., 2015) and those indicated by the Nd isotope records. Furthermore, changes in interhemispheric coupling between the monsoon systems and southern-sourced intermediate water formation between different background climate states may represent an important component of the atmosphere-ocean-climate system that deserves further in-depth investigation in future observational and modeling efforts.

## Data Availability Statement

The data from this study are available at Zenodo (<https://zenodo.org/record/6400091>) and also in the supporting materials.

## Acknowledgments

This study was supported by the Strategic Priority Research Program of Chinese Academy of Sciences (XDB42010402), the National Natural Science Foundation of China (91958107 and 41806060), Youth Innovation Promotion Association, CAS (2020210), Laboratory for Marine Geology, Qingdao Pilot National Laboratory for Marine Science and Technology (MGQNLMTD201902), National Research Agency MONOPOL project (ANR 2011 Blanc SIMI 5–6 024 04), and the Key Deployment Project of CAS Centre for Ocean Mega-Science (COMS2019Q07). DJW is supported by a Natural Environment Research Council independent research fellowship (NE/T011440/1). We thank Jiaoyang Ruan, Jianghui Du and Xu Zhang for helpful discussions and several reviewers for their insightful comments.

## References

- Abbott, A., Lühr, S., Payne, A., Kumar, H., & Du, J. (2022). Widespread lithogenic control of marine authigenic neodymium isotope records? Implications for paleoceanographic reconstructions. *Geochimica et Cosmochimica Acta*, 319, 318–336. <https://doi.org/10.1016/j.gca.2021.11.021>
- Ahmad, S. M., Padmakumari, V., & Babu, G. A. (2009). Strontium and neodymium isotopic compositions in sediments from Godavari, Krishna, and Pennar rivers. *Current Science*, 97(12).
- Amakawa, H., Yu, T.-L., Tazoe, H., Obata, H., Gamo, T., Sano, Y., et al. (2019). Neodymium concentration and isotopic composition distributions in the southwestern Indian Ocean and the Indian sector of the Southern Ocean. *Chemical Geology*, 511, 190–203. <https://doi.org/10.1016/j.chemgeo.2019.01.007>
- Anderson, R. F., Ali, S., Bradtmiller, L. I., Nielsen, S. H. H., Fleisher, M. Q., Anderson, B. E., & Burckle, L. H. (2009). Wind-driven upwelling in the Southern Ocean and the deglacial rise in atmospheric CO<sub>2</sub>. *Science*, 323(5920), 1443–1448. <https://doi.org/10.1126/science.1167441>
- Basak, C., Martin, E. E., Horikawa, K., & Marchitto, T. M. (2010). Southern Ocean source of <sup>14</sup>C-depleted carbon in the North Pacific Ocean during the last deglaciation. *Nature Geoscience*, 3(11), 770–773. <https://doi.org/10.1038/ngeo987>
- Blaser, P., Pöppelmeier, F., Schulz, H., Gutjahr, M., Frank, M., Lippold, J., et al. (2019). The resilience and sensitivity of Northeast Atlantic deep water eNd to overprinting by detrital fluxes over the past 30,000 yr. *Geochimica et Cosmochimica Acta*, 245, 79–97. <https://doi.org/10.1016/j.gca.2018.10.018>
- Bolton, C. T., Chang, L., Clemens, S. C., Kodama, K., Ikehara, M., Medina-Elizalde, M., et al. (2013). A 500,000 yr record of Indian Summer Monsoon dynamics recorded by eastern equatorial Indian Ocean upper water-column structure. *Quaternary Science Reviews*, 77, 167–180. <https://doi.org/10.1016/j.quascirev.2013.07.031>
- Bryan, S. P., Marchitto, T. M., & Lehman, S. J. (2010). The release of <sup>14</sup>C-depleted carbon from the deep ocean during the last deglaciation: Evidence from the Arabian Sea. *Earth and Planetary Science Letters*, 298(1–2), 244–254. <https://doi.org/10.1016/j.epsl.2010.08.025>
- Burton, K. W., & Vance, D. (2000). Glacial-interglacial variations in the neodymium isotope composition of seawater in the Bay of Bengal recorded by planktonic foraminifera. *Earth and Planetary Science Letters*, 176(3), 425–441. [https://doi.org/10.1016/S0012-821X\(00\)00011-X](https://doi.org/10.1016/S0012-821X(00)00011-X)
- Caley, T., Malaizé, B., Zaragosi, S., Rossignol, L., Bourget, J., Eynaud, F., et al. (2011). New Arabian Sea records help decipher orbital timing of Indo-Asian monsoon. *Earth and Planetary Science Letters*, 308(3), 433–444. <https://doi.org/10.1016/j.epsl.2011.06.019>
- Cheng, H., Edwards, R. L., Sinha, A., Spötl, C., Yi, L., Chen, S., et al. (2016). The Asian monsoon over the past 640,000 yr and ice age terminations. *Nature*, 534(7609), 640–646. <https://doi.org/10.1038/nature18591>
- Clemens, S. C., & Prell, W. L. (2003). A 350,000 yr summer-monsoon multi-proxy stack from the Owen Ridge, Northern Arabian Sea. *Marine Geology*, 201(1), 35–51. [https://doi.org/10.1016/S0025-3227\(03\)00207-X](https://doi.org/10.1016/S0025-3227(03)00207-X)
- Comas-Bru, L., Atsawawanunt, K., & Harrison, S. (2020). SISAL (Speleothem Isotopes Synthesis and Analysis Working Group) database, version 2.0.
- Conterras-Rosales, L. A., Jennerjahn, T., Tharammal, T., Meyer, V., Lückge, A., Paul, A., & Schefuß, E. (2014). Evolution of the Indian Summer Monsoon and terrestrial vegetation in the Bengal region during the past 18 ka. *Quaternary Science Reviews*, 102(102), 133–148. <https://doi.org/10.1016/j.quascirev.2014.08.010>
- Deplazes, G., Lückge, A., Stuut, J.-B. W., Pätzold, J., Kuhlmann, H., Husson, D., et al. (2014). Weakening and strengthening of the Indian monsoon during Heinrich events and Dansgaard-Oeschger oscillations. *Paleoceanography*, 29(2), 99–114. <https://doi.org/10.1002/2013pa002509>
- Dessert, C., Dupré, B., François, L. M., Schott, J., Gaillardet, J., Chakrapani, G., & Bajpai, S. (2001). Erosion of Deccan Traps determined by river geochemistry: Impact on the global climate and the <sup>87</sup>Sr/<sup>86</sup>Sr ratio of seawater. *Earth and Planetary Science Letters*, 188(3), 459–474. [https://doi.org/10.1016/S0012-821X\(01\)00317-X](https://doi.org/10.1016/S0012-821X(01)00317-X)
- Dutt, S., Gupta, A. K., Clemens, S. C., Cheng, H., Singh, R. K., Kathayat, G., & Edwards, R. L. (2015). Abrupt changes in Indian Summer Monsoon strength during 33,800–5,500 yr B.P. *Geophysical Research Letters*, 42(13), 5526–5532. <https://doi.org/10.1002/2015gl064015>
- Foster, G. L., & Vance, D. (2006). Negligible glacial-interglacial variation in continental chemical weathering rates. *Nature*, 444(7121), 918–921. <https://doi.org/10.1038/nature05365>

- Galy, A., & France-Lanord, C. (2001). Higher erosion rates in the Himalaya: Geochemical constraints on riverine fluxes. *Geology*, 29(1), 23–26. [https://doi.org/10.1130/0091-7613\(2001\)029<0023:herith>2.0.co;2](https://doi.org/10.1130/0091-7613(2001)029<0023:herith>2.0.co;2)
- Goldstein, S. L., & Hemming, S. R. (2003). Long-lived isotopic tracers in oceanography, paleoceanography, and ice-sheet dynamics. *Treatise on Geochemistry*, 6, 625. <https://doi.org/10.1016/b0-08-043751-6/06179-x>
- Goswami, V., Singh, S. K., & Bhushan, R. (2014). Impact of water mass mixing and dust deposition on Nd concentration and  $\epsilon_{Nd}$  of the Arabian Seawater column. *Geochimica et Cosmochimica Acta*, 145, 30–49. <https://doi.org/10.1016/j.gca.2014.09.006>
- Goswami, V., Singh, S. K., Bhushan, R., & Rai, V. K. (2012). Temporal variations in  $^{87}Sr/^{86}Sr$  and  $\epsilon Nd$  in sediments of the southeastern Arabian Sea: Impact of monsoon and surface water circulation. *Geochemistry, Geophysics, Geosystems*, 13(1). <https://doi.org/10.1029/2011gc003802>
- Gourlan, A. T., Meynadier, L., Allègre, C. J., Tapponnier, P., Birck, J.-L., & Joron, J.-L. (2010). Northern Hemisphere climate control of the Bengali rivers discharge during the past 4 Ma. *Quaternary Science Reviews*, 29(19), 2484–2498. <https://doi.org/10.1016/j.quascirev.2010.05.003>
- Groottes, P. M., & Stuiver, M. (1997). Oxygen 18/16 variability in Greenland snow and ice with  $10^3$ – $10^5$  yr time resolution. *Journal of Geophysical Research: Oceans*, 102(C12), 26455–26470. <https://doi.org/10.1029/97jc00880>
- Hein, C. J., Galy, V., Galy, A., France-Lanord, C., Kudrass, H., & Schwenk, T. (2017). Post-glacial climate forcing of surface processes in the Ganges-Brahmaputra river basin and implications for carbon sequestration. *Earth and Planetary Science Letters*, 478, 89–101. <https://doi.org/10.1016/j.epsl.2017.08.013>
- Hillenbrand, C.-D., Smith, J. A., Hodell, D. A., Greaves, M., Poole, C. R., Kender, S., et al. (2017). West Antarctic Ice Sheet retreat driven by Holocene warm water incursions. *Nature*, 547(7661), 43–48. <https://doi.org/10.1038/nature22995>
- Hu, R., Noble, T. L., Piotrowski, A. M., Mccave, I. N., Bostock, H. C., & Neil, H. L. (2016). Neodymium isotopic evidence for linked changes in southeast Atlantic and southwest Pacific circulation over the last 200 kyr. *Earth and Planetary Science Letters*, 455, 106–114. <https://doi.org/10.1016/j.epsl.2016.09.027>
- Kathayat, G., Cheng, H., Sinha, A., Spötl, C., Edwards, R. L., Zhang, H., et al. (2016). Indian monsoon variability on millennial-orbital timescales. *Scientific Reports*, 6, 24374. <https://doi.org/10.1038/srep24374>
- Kaushal, N., Breitenbach, S. F., Lechleitner, F. A., Sinha, A., Tewari, V. C., Ahmad, S. M., et al. (2018). The Indian Summer Monsoon from a speleothem  $\delta^{18}O$  perspective—A review. *Quaternary*, 1(3), 29. <https://doi.org/10.3390/quat1030029>
- Kudrass, H. R., Hofmann, A., Doose, H., Emeis, K., & Erlenkeuser, H. (2001). Modulation and amplification of climatic changes in the Northern Hemisphere by the Indian Summer Monsoon during the past 80 k.y. *Geology*, 29(1), 63–66. [https://doi.org/10.1130/0091-7613\(2001\)029<0063:maaocc>2.0.co;2](https://doi.org/10.1130/0091-7613(2001)029<0063:maaocc>2.0.co;2)
- Laskar, J., Robutel, P., Joutel, F., Gastineau, M., Correia, A., & Levrard, B. (2004). A long-term numerical solution for the insolation quantities of the Earth. *Astronomy & Astrophysics*, 428(1), 261–285. <https://doi.org/10.1051/0004-6361:20041335>
- Lenard, S. J. P., Lavé, J., France-Lanord, C., Aumaître, G., & Keddadouche, K. (2020). Steady erosion rates in the Himalayas through late Cenozoic climatic changes. *Nature Geoscience*, 13(6), 1–5. <https://doi.org/10.1038/s41561-020-0585-2>
- Lightfoot, P., & Hawkesworth, C. (1988). Origin of Deccan Trap lavas: Evidence from combined trace element and Sr-, Nd- and Pb-isotope studies. *Earth and Planetary Science Letters*, 91(1), 89–104. [https://doi.org/10.1016/0012-821x\(88\)90153-7](https://doi.org/10.1016/0012-821x(88)90153-7)
- Liu, X., Liu, J., Chen, S., Chen, J., Zhang, X., Yan, J., & Chen, F. (2020). New insights on Chinese cave  $\delta^{18}O$  records and their paleoclimatic significance. *Earth-Science Reviews*, 207, 103216. <https://doi.org/10.1016/j.earscirev.2020.103216>
- Lupker, M., France-Lanord, C., Galy, V., Lavé, J., & Kudrass, H. (2013). Increasing chemical weathering in the Himalayan system since the last glacial maximum. *Earth and Planetary Science Letters*, 365, 243–252. <https://doi.org/10.1016/j.epsl.2013.01.038>
- Marchitto, T. M., Lehman, S. J., Ortiz, J. D., Flückiger, J., & Van, G. A. (2007). Marine radiocarbon evidence for the mechanism of deglacial atmospheric CO<sub>2</sub> rise. *Science*, 316(5830), 1456. <https://doi.org/10.1126/science.1138679>
- McManus, J. F., Francois, R., Gherardi, J. M., Keigwin, L. D., & Brown-Leger, S. (2004). Collapse and rapid resumption of Atlantic meridional circulation linked to deglacial climate changes. *Nature*, 428(6985), 834–837. <https://doi.org/10.1038/nature02494>
- Miriyala, P., Sukumaran, N. P., Nath, B. N., Ramamurthy, P. B., Sijinkumar, A. V., Vijayagopal, B., et al. (2017). Increased chemical weathering during the deglacial to mid-Holocene summer monsoon intensification. *Scientific Reports*, 7, 44310. <https://doi.org/10.1038/srep44310>
- Naik, S. S., Basak, C., Goldstein, S. L., Naidu, P. D., & Naik, S. N. (2019). A 16 kyr record of ocean circulation and monsoon intensification from the Central Bay of Bengal. *Geochemistry, Geophysics, Geosystems*, 20(2), 872–882. <https://doi.org/10.1029/2018gc007860>
- Nilsson-Kerr, K., Anand, P., Sexton, P. F., Leng, M. J., Misra, S., Clemens, S. C., & Hammond, S. J. (2019). Role of Asian summer monsoon subsystems in the inter-hemispheric progression of deglaciation. *Nature Geoscience*, 12(4), 290–295. <https://doi.org/10.1038/s41561-019-0319-5>
- Perera, L., & Kagami, H. (2011). Centimeter- and meter-scale Nd and Sr isotopic homogenization in Kadugannawa complex, Sri Lanka. *Journal of the Geological Society of Sri Lanka*, 14, 129–141.
- Singh, S. K., & France-Lanord, C. (2002). Tracing the distribution of erosion in the Brahmaputra watershed from isotopic compositions of stream sediments. *Earth and Planetary Science Letters*, 202(3), 645–662. [https://doi.org/10.1016/s0012-821x\(02\)00822-1](https://doi.org/10.1016/s0012-821x(02)00822-1)
- Tachikawa, K., Piotrowski, A. M., & Bayon, G. (2014). Neodymium associated with foraminiferal carbonate as a recorder of seawater isotopic signatures. *Quaternary Science Reviews*, 88, 1–13. <https://doi.org/10.1016/j.quascirev.2013.12.027>
- Talley, L. D. (1996). Antarctic Intermediate Water in the South Atlantic. In *The South Atlantic: Present and past circulation* (pp. 219–238). Berlin, Heidelberg: Springer Berlin Heidelberg. [https://doi.org/10.1007/978-3-642-80353-6\\_11](https://doi.org/10.1007/978-3-642-80353-6_11)
- Tierney, J. E., Pausata, F. S. R., & de Menocal, P. (2015). Deglacial Indian monsoon failure and North Atlantic stadials linked by Indian Ocean surface cooling. *Nature Geoscience*, 9, 46. <https://doi.org/10.1038/ngeo2603>
- Vance, D., Teagle, D. A. H., & Foster, G. L. (2009). Variable Quaternary chemical weathering fluxes and imbalances in marine geochemical budgets. *Nature*, 458, 493. <https://doi.org/10.1038/nature07828>
- van de Flierdt, T., Griffiths, A. M., Lambelet, M., Little, S. H., Stichel, T., & Wilson, D. J. (2016). Neodymium in the oceans: A global database, a regional comparison and implications for paleoceanographic research. *Philosophical Transactions of the Royal Society A*, 374(2081), 20150293. <https://doi.org/10.1098/rsta.2015.0293>
- von Blanckenburg, F., Bouchez, J., Ibarra, D. E., & Maher, K. (2015). Stable runoff and weathering fluxes into the oceans over Quaternary climate cycles. *Nature Geoscience*, 8, 538. <https://doi.org/10.1038/ngeo2452>
- WAIS Divide Project Members. (2013). Onset of deglacial warming in West Antarctica driven by local orbital forcing. *Nature*, 500(7463), 440–444.
- Willenbring, J. K., & von Blanckenburg, F. (2010). Long-term stability of global erosion rates and weathering during late-Cenozoic cooling. *Nature*, 465(7295), 211–214. <https://doi.org/10.1038/nature09044>
- Wilson, D. J., Galy, A., Piotrowski, A. M., & Banakar, V. K. (2015). Quaternary climate modulation of Pb isotopes in the deep Indian Ocean linked to the Himalayan chemical weathering. *Earth and Planetary Science Letters*, 424, 256–268. <https://doi.org/10.1016/j.epsl.2015.05.014>
- Wilson, D. J., Piotrowski, A. M., Galy, A., & Banakar, V. K. (2015). Interhemispheric controls on deep ocean circulation and carbon chemistry during the last two glacial cycles. *Paleoceanography*, 30(6), 621–641. <https://doi.org/10.1002/2014pa002707>

- Wilson, D. J., Piotrowski, A. M., Galy, A., & McCave, I. N. (2012). A boundary exchange influence on deglacial neodymium isotope records from the deep western Indian Ocean. *Earth and Planetary Science Letters*, *341*, 35–47. <https://doi.org/10.1016/j.epsl.2012.06.009>
- Yu, Z., Colin, C., Ma, R., Meynadier, L., Wan, S., Wu, Q., et al. (2018). Antarctic Intermediate Water penetration into the northern Indian Ocean during the last deglaciation. *Earth and Planetary Science Letters*, *500*, 67–75. <https://doi.org/10.1016/j.epsl.2018.08.006>
- Yu, Z., Colin, C., Meynadier, L., Douville, E., Dapoigny, A., Reverdin, G., et al. (2017). Seasonal variations in dissolved neodymium isotope composition in the Bay of Bengal. *Earth and Planetary Science Letters*, *479*, 310–321. <https://doi.org/10.1016/j.epsl.2017.09.022>
- Zhao, N., Oppo, D. W., Huang, K. F., Howe, J. N. W., & Keigwin, L. D. (2019). Glacial-interglacial Nd isotope variability of North Atlantic Deep Water modulated by North American ice sheet. *Nature Communications*, *10*(1), 5773. <https://doi.org/10.1038/s41467-019-13707-z>